


論文 / 著書情報
Article / Book Information

Title	Seasonal sea breeze variation analysis based on multi-year near-surface observations in Jakarta, Indonesia
Authors	I Dewa Gede Agung Junnaedhi, Atsushi Inagaki, Rezza Ferdiansyah Muhammad, Manabu Kanda
Citation	International Journal of Climatology, vol. 43, Issue 11, p. 5177-5195
Pub. date	2023, 6
DOI	https://doi.org/10.1002/joc.8139
Creative Commons	Information is in the article.

RESEARCH ARTICLE

Seasonal sea breeze variation analysis based on multi-year near-surface observations in Jakarta, Indonesia

I Dewa Gede Agung Junnaedhi^{1,2}  | Atsushi Inagaki¹ |
Muhammad Rezza Ferdiansyah³ | Manabu Kanda¹

¹Department of Transdisciplinary Science and Engineering, Tokyo Institute of Technology, Tokyo, Japan

²Atmospheric Sciences Research Group, Faculty of Earth Sciences and Technology, Institut Teknologi Bandung, Bandung, Indonesia

³Center for Public Weather Services, Badan Meteorologi Klimatologi dan Geofisika, Jakarta, Indonesia

Correspondence

I Dewa Gede Agung Junnaedhi,
Department of Transdisciplinary Science and Engineering, Tokyo Institute of Technology, Tokyo, Japan.
Email: junnaedhi.i.aa@m.titech.ac.jp

Funding information

Indonesian Endowment Fund (Lembaga Pengelola Dana Beasiswa - LPDP) scholarship; Japan Society for Promotional of Science (JSPS) KAKENHI grants, Grant/Award Numbers: 21H04573, 19KK0105

Abstract

In this study, multi-year near-surface observations were conducted at two sites in Jakarta, Indonesia to analyse seasonal sea breeze variation. Seasonal length was defined using observed zonal wind components, the rainy season was defined as December–March, and the dry season was defined as May–September. We found that the sea breeze in Jakarta started earlier, propagated more rapidly, and lasted for a shorter period of time during the rainy than dry season. Variation in the air temperature difference between urban and coastal areas of Jakarta was the major factor driving sea breeze seasonal variation. During the rainy season, night-time cloud downwelling decreased this air temperature difference, causing earlier sea breeze onset and more rapid sea breeze propagation due to a weaker land breeze. By contrast, during the dry season, intense night-time radiative cooling inland caused a strong negative temperature difference that produced a stronger land breeze, thus, slowing sea breeze propagation. Seasonal differences in urban surface heating and urban heat island circulation may also affect sea breeze onset and propagation speed. Discrepancies in thermal properties between urban core and coastal areas of Jakarta also prolonged positive temperature differences after sunset, thus extending the sea breeze duration in the dry season.

KEYWORDS

Jakarta, multi-year surface observation, propagation speed, sea breeze, seasonal variation

1 | INTRODUCTION

Near-surface atmospheric conditions are influenced by a complex combination of various phenomena from micro- to global scales. Coupling between annual and diurnal circulation patterns is a fundamental driver of weather and climate systems in the Maritime Continent (MC) (Nitta & Sekine, 1994; Qian et al., 2010; Yamanaka, 2016; Yang &

Slingo, 2001). Both circulation patterns are in turn driven by variations in solar forcing, arising as a consequence of the annual march of the sun and Earth's rotation, respectively. Annual circulation of monsoon, which govern MC's seasonal transition (Chang, Wang, et al., 2005b; Hamada et al., 2002; Yoden et al., 2016), may exert some control on the diurnal circulation. On the other hand, diurnal circulations in the MC also have a strong teleconnection to the

This is an open access article under the terms of the [Creative Commons Attribution-NonCommercial](https://creativecommons.org/licenses/by-nc/4.0/) License, which permits use, distribution and reproduction in any medium, provided the original work is properly cited and is not used for commercial purposes.

© 2023 The Authors. *International Journal of Climatology* published by John Wiley & Sons Ltd on behalf of Royal Meteorological Society.

global climate through the distribution of heat and moisture via global atmospheric circulation (Yang & Slingo, 2001). Diurnal circulation, particularly sea breeze, may be the most important variable influencing the MC climate (Yamanaka et al., 2018).

Seasonal variation in land–sea–air temperature difference and background wind will induce variation in sea breeze (Azorin-Molina et al., 2011; Gilliam et al., 2004; Grau et al., 2021; Shen et al., 2021). Variation in sea breeze onset, cessation, and duration were observed in the monsoonal region of the eastern Indian (Reddy et al., 2021). In the MC, specifically over the eastern coast of the Malay Peninsula, the seasonal change in cloudiness is the most important factor that affect sea breeze onset and strength (Jayakrishnan et al., 2021). Seasonal variation of sea breeze can also be induced by the physical settings of sea breeze path (Gilliam et al., 2004; Miller et al., 2003). One important of such physical setting is the existence of city or urban area. Urban area development and urbanization could modify the sea breeze frequency and characteristics, although this modification may be varied between cities. In Shanghai, for example, increased urban roughness and decreased solar radiation by anthropogenic aerosol are assumed to cause reduction of summer sea breeze frequency and wind speed (Shen et al., 2019). In Adelaide, however, temperature increase and urban heat island (UHI) due to urbanization are considered as the cause of increase in sea breeze maximum wind speed and sea breeze earlier onset, notably during summer and autumn (Masouleh et al., 2019). UHI circulation, a phenomena commonly occurs in large cities, may interact with sea breeze and modify its characteristics (Cenedese & Monti, 2003; Freitas et al., 2007; Hu et al., 2022; Hu & Xue, 2016; Yoshikado & Kondo, 1989). Due to this interaction, seasonal differences in UHI intensity, could potentially alter the sea breeze onset and propagation speed (Wang et al., 2019; Yoshikado, 1992). Such seasonal differences in UHI-intensity in MC's tropical city have been demonstrated through extensive observation in Singapore (Chow & Roth, 2006; Roth et al., 2022). Their result shows consistently higher UHI intensity during dry season compared to rainy season. Thus, it is important to consider the urban influences into the seasonal variation of sea breeze.

Atmospheric conditions in Jakarta, Indonesia, which is the largest megacity in the MC, are strongly influenced by the sea breeze in both the dry and rainy seasons. During the dry season, the sea breeze is the main driver of aerosol and pollutant transport (Pinandito et al., 2001; Sofyan et al., 2007), whereas during the rainy season, the sea breeze may trigger afternoon precipitating clouds, especially in southern Jakarta (Renggono et al., 2001). Observations have suggested that sea and land breeze

circulation are the main drivers of the meridional migration of diurnal rainfall between Jakarta coastal and southern inland areas (Mori et al., 2018). On the other hand, urban area and urban development in Jakarta may change the sea breeze. A recent study suggests that the UHI may be causing the delay of sea breeze propagation over Jakarta (Ferdiansyah et al., 2020), and such change could affect the timing and strength of convective storm (Robinson et al., 2013). Numerical simulation by Argüeso et al. (2016) has shown that the existence of the city of Jakarta will enhance sea breeze circulations, increase near-surface moisture flux convergence, and lead to an increase of precipitation.

Due to the importance of sea breeze for Jakarta, it is necessary to understand how it varies over the seasons and whether the city affects this variation. A boundary-layer radar (BLR) study conducted in Serpong, a suburb of Jakarta, showed that a clear sea breeze signal is usually found during the dry season, but not in the rainy season (Hadi et al., 2002). They also show that sea breeze intrusion occurred earlier on cloudy days; however, the mechanism was not investigated. Using the same dataset, a later study observed sea breeze circulation during the rainy season, especially when the prevailing winds were weak (Araki et al., 2006). Although seasonal variation in sea breeze intensity has been discussed, seasonal variation in sea breeze onset, duration, and propagation has not yet been studied in Jakarta; such an analysis requires long-term observations collected at multiple locations.

The objective of this study is to extend our knowledge of sea breeze characteristics in Jakarta, focusing on its seasonal variation of onset, duration, and propagation speed. Using a multi-year dataset obtained from two near-surface observation stations in Jakarta, we examined the effects of seasonal transition on the sea breeze and explored the potential underlying mechanism. This study is the first to observe sea breeze characteristics within the urban area of Jakarta. Our findings will provide a foundation for future studies on interactions between the sea breeze and climate change and/or urbanization in Jakarta. Microclimate changes observed in Jakarta (Siswanto et al., 2022) may also influence the sea breeze (Darmanto et al., 2019); therefore, knowledge about seasonal sea breeze variation will be important for isolating the effects of climate change and urbanization, thus improving the accuracy of future analyses.

2 | THEORETICAL BACKGROUND

The sea breeze is a shallow layer of cool, moist marine air that moves inland in response to local-scale pressure differences between sea and land during the daytime

(Miller et al., 2003). The sea breeze is a component of mesoscale circulation, along with landward lower flow, rising flow inland, seaward upper flow, and sinking air over the sea at distances of several kilometres from the shore. The lower part of this circulation pattern is a gravity-driven current generated by density differences between sea and land due to differential temperatures (Simpson & Britter, 1979). The leading edge of this gravity current, that is, the interface between the marine and land air masses, also known as the sea breeze front (SBF), is usually characterized by sharp changes in wind speed, humidity, and temperature. The sea breeze propagation speed (V_{SBF}) is the speed at which the SBF migrates, and is differentiated from the sea breeze wind speed. The sea breeze structure is described in detail elsewhere (Miller et al., 2003).

The sea breeze is a gravity-driven current (Simpson, 1969; Simpson & Britter, 1979) with a propagation speed or densimetric speed (V_d) calculated as follows:

$$V_d = k \sqrt{\frac{\rho_2 - \rho_1}{\rho_1} gh} = k \sqrt{\frac{\Delta \rho}{\rho_1} gh}. \quad (1)$$

where ρ_1 ($\text{kg} \cdot \text{m}^{-3}$) is the density of the lighter land air mass, ρ_2 ($\text{kg} \cdot \text{m}^{-3}$) is that of the denser marine air mass, g is acceleration due to gravity ($9.8 \text{ m} \cdot \text{s}^{-2}$), h (m) is the depth of the current or denser air, and k is the internal Froude number, which represents the ratio between the inertial and buoyancy forces. Because density is inversely proportional to temperature (T), Equation (1) can be rearranged as:

$$V_d = k \sqrt{\frac{\Delta T}{T} gd}, \quad (2)$$

where ΔT (K) is the temperature difference between the land air and marine air masses, and T (K) is the absolute temperature of the denser air mass (Miller et al., 2003; Schoenberger, 1984; Simpson, 1969). The V_d can be considered as the propagation speed of a dense air mass into lighter ambient air in the absence of opposing flow. The presence of a flow in ambient air (V_g) will reduce or increase the gravity current propagation; such a flow may be caused by a cross-shore geostrophic wind component resulting from a synoptic scale pressure gradient or the opposing land breeze flow. Based on the correlation between experimental and atmospheric data, Simpson and Britter (1980) estimated that an opposing flow would reduce the V_d of a sea breeze by 3/5 of its strength, and estimated an optimal k of approximately 0.87. A rough estimate of the V_{SBF} is given by:

$$V_{\text{SBF}} = 0.87 \sqrt{\frac{\Delta T}{T} gd} - 0.59 V_g. \quad (3)$$

Thus, in the absence of an opposing flow, $V_{\text{SBF}} = V_d$, and is in the range $1\text{--}5 \text{ m} \cdot \text{s}^{-1}$ (Stull, 1988).

It is clear from Equation (3) that the sea breeze gravity current will be initiated when there is a positive temperature difference between air masses over land and sea (ΔT). Conversely, the sea breeze current will cease when the temperature over land drops below that over the sea, that is, ΔT will become negative. The time between sea breeze onset and cessation is the sea breeze duration, which depends on the length of time that ΔT remains positive.

3 | DATASET

The main dataset used in this study comprised near-surface observations conducted at two sites in urban areas of Jakarta. Jakarta is located on the northern coast of western Java Island (Figure 1). Along its northern side, its width is the same as that of Jakarta Bay ($\sim 30 \text{ km}$), whereas its southern side has a width of only $\sim 13 \text{ km}$. The distance from Jakarta Bay to the southern border is $\sim 30 \text{ km}$. Jakarta is located in a relatively flat area, with a mountain range $\sim 50 \text{ km}$ to the south having a maximum height of 3000 m a.s.l. (Mt. Gede-Pangrango).

The main dataset was used to characterize the sea breeze and analysed to obtain the seasonal variation in sea breeze onset, duration, and propagation speed. We also used several freely available datasets in our analysis.

3.1 | Near-surface observations

Meteorological observations were conducted at two sites in Jakarta (Figure 1a). The sites were selected for ease of sea breeze propagation measurement. The first observation site is a coastal area $\sim 450 \text{ m}$ from the Jakarta coast. The instruments were placed on top of a building owned by Badan Riset Kelautan dan Perikanan–Kementrian Kelautan dan Perikanan (KKP), hereinafter KKP. There are many residential houses to the east of the site, a highway to the south, and a recreational area to the west (Figure 1a, inset). The KKP building is 18 m in height, which is higher than most surrounding structures, except for an apartment building to the north–northwest. All instruments were mounted on 2-m steel poles, as shown in Figure 1b.

The second site is in the business district in the urban core of Jakarta, 11.26 km to the south of the KKP

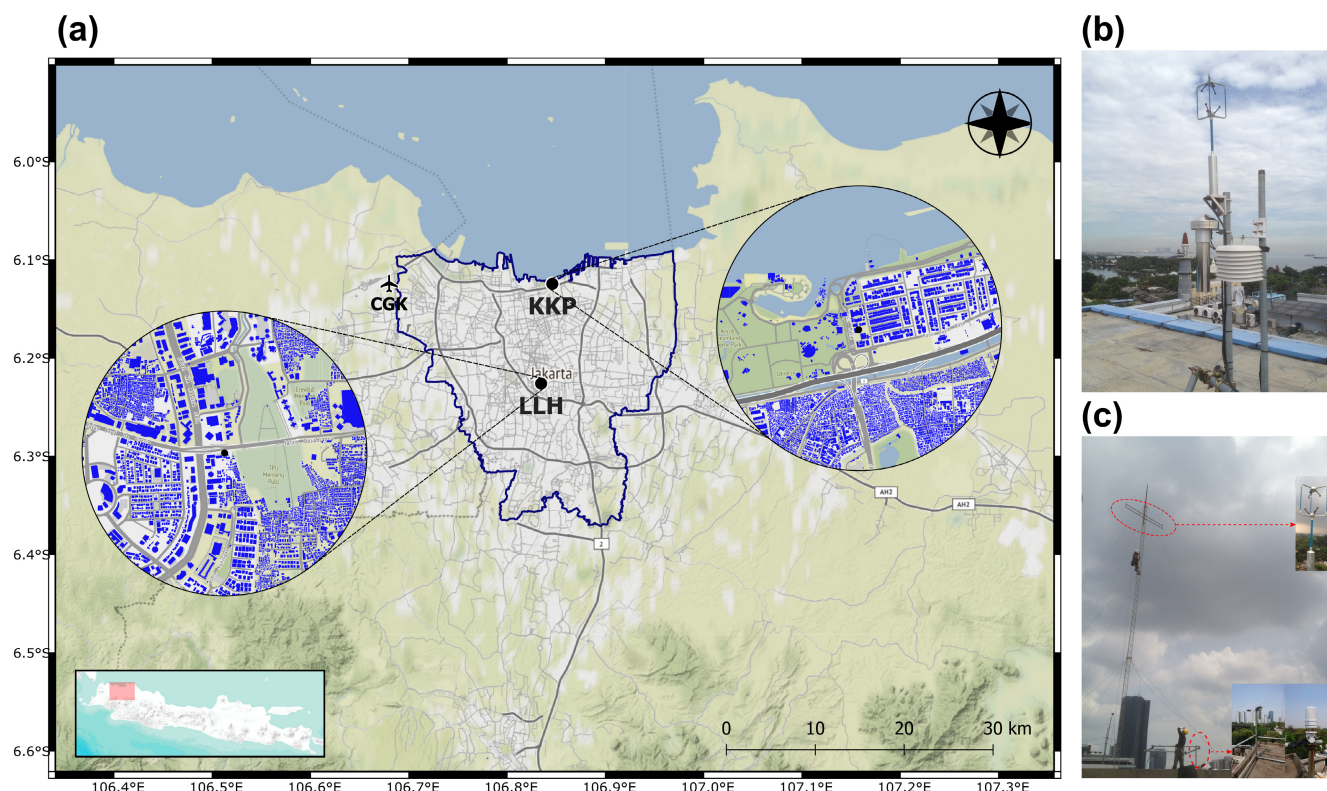


FIGURE 1 (a) Map of Jakarta, Indonesia showing observation sites; and photographs of the observation instruments used at the (b) Kementrian Kelautan dan Perikanan (KKP) and (c) Laboratorium Lingkungan Hidup (LLH) sites. In (a), the sounding station at Soekarno-Hatta International Airport (CGK) is indicated by the plane symbol; and the perimeter line indicates the Jakarta city administrative boundary. Building footprints within a 1-km radius of the observation sites are shown in the circular inset. The rectangular inset shows a map of Java Island indicating the position of the study area. The base map was designed using a relief map obtained from Stamen Design (<http://maps.stamen.com/terrain>). [Colour figure can be viewed at wileyonlinelibrary.com]

building. Instruments were placed on top of a building owned by Laboratorium Lingkungan Hidup (LLH), Jakarta City Government, hereinafter LLH. The LLH building has a height of 22 m, which is extended by a 10-m lattice tower. There is a large cemetery to the east of the park, and many tall buildings to the north and southwest. Wind and radiation measurement instruments were mounted on the lattice tower at a height 7.3 m above the rooftop, and other instruments were mounted at the base of the tower (Figure 1c). A detailed description of the site is provided in Table 1. Because the instruments were mounted on the tops of buildings, we considered the observations to have been collected within the urban roughness sublayer (Oke et al., 2017).

The main instruments used at both sites were ultrasonic anemometers and temperature/humidity gauges (Figure 1b, c). A net radiometer and automatic weather station (AWS) were also installed on the LLH building. The main purpose of the AWS was to obtain rainfall data for ultrasonic anemometer screening. Measurements were mainly logged at a sampling rate of 10 Hz, whereas the net radiometer and AWS logged measurements at 1- and 5-min intervals, respectively. Detail specification of

the instruments is presented in Table 2. Observations were conducted from March 2017 to October 2021, except for net radiometer measurements, which started in January 2019. Data were not obtained continuously throughout the observation period; they could not be obtained during several periods due to errors or technical problems. At the LLH building, no data were obtained for nearly 5 months, from June to October, 2020. Approximately 45 months of data were obtained for the analysis.

3.2 | Data processing

The average of each observed variable was used for the analysis. Averaged 1-h variables were mainly analysed, with 10-min averages used to identify sea breeze intrusion and cessation. Prior to averaging, observation data from the main instruments were subjected to pre-processing. Thresholds of $\pm 25 \text{ m} \cdot \text{s}^{-1}$, 278.15–318.15 K, and 0%–100% were used to detect non-physical wind speed components (U , V , W), air temperature (T), and relative humidity (RH), respectively. Anomalously high or low measurements within very short periods, that is,

TABLE 1 Descriptions of the observation sites.

Description	KKP	LLH
Building height	18 m	22 m
Terrain elevation	2.9 m	13.6 m
Site surrounding	Coastal area, ± 450 m from sea, with large recreational area with dense vegetation in northwest (NW) to southwest (SW) direction. Building base higher than surrounding canopy, except for one building in the north	Business district in urban core area, with many tall buildings in north (N) and southwest (SW) direction. There is a large cemetery in north-northeast (NNE) to south-southeast (SSE) direction with sparse vegetation.
Measurement height (z_m)	ultrasonic anemometer: 21 m temperature/humidity gauge: 20 m	ultrasonic anemometer: 29.3 m net radiometer: 29.3 m temperature/humidity gauge: 23 m automatic weather station: 23 m
Displacement height (z_d) *) Darmanto et al. (2017)	13.5 m	12.8 m

Abbreviations: LLH, Laboratorium Lingkungan Hidup; KKP, Kementerian Kelautan dan Perikanan.

spikes, were detected using the median absolute deviation (MAD) algorithm (Mauder et al., 2013). Observation sample x_i is considered a spike if its absolute value ($|x_i|$) is larger than $|\langle x \rangle \pm \frac{7 \times \text{MAD}}{0.6745}|$, where $\langle x \rangle$ symbolizing the median of x and $\text{MAD} = \langle |x_i - \langle x \rangle| \rangle$. Erroneous measurements were replaced with values linearly interpolated from adjacent measurements, or with average values of non-erroneous measurements, depending on the number of consecutive erroneous measurements. If the proportion of erroneous measurements exceeded 60% of the total sample window, the average value was discarded. Because ultrasonic anemometers are highly sensitive to rain, we 'screened' variables measured by this instrument using AWS rainfall intensity data, at a threshold of $\geq 1 \text{ mm h}^{-1}$. The total amount of data that was removed by the rainfall-threshold is 5.2% at KKP and 6.1% at LLH. After processing and screening, from all 1-h mean values

between 1st March 2017 0000 and 31st October 2021 2300, usable data acquired is 82.5% and 74.3% from KKP and LLH sites, respectively.

Although average values were the main focus, we also examined wind fluctuations (u', v', w') and sonic temperature (T_s') to calculate sensible heat flux (Q_H) and stability parameter (ζ). Sensible heat flux is calculated as follows:

$$Q_H = \rho C_p \overline{w' T_s'}, \quad (4)$$

where ρ is the air density, C_p is the specific heat of air at constant pressure, and $\overline{w' T_s'}$ is the covariance of w and T_s' (Stull, 1988). The stability parameter is calculated from effective height (z) and Obukhov length (L) as follows:

$$\zeta = \frac{z}{L} = \frac{(z_m - z_d)}{\left[\frac{T_s u_*^3}{kg w' T_s'} \right]} \quad (5)$$

where z_m measurement height, z_d is displacement height, k is von Karman constant (0.4), and u_* is friction velocity, which is estimated using:

$$u_* = \sqrt[4]{(\overline{u'w'})^2 + (\overline{v'w'})^2}. \quad (6)$$

The displacement height (z_d) is obtained from estimation by Darmanto et al. (2017). The value of z_m and z_d are tabulated in Table 1.

3.3 | Support datasets

To support our analyses, we retrieved several openly available datasets. Sounding data observed by Badan Meteorologi Klimatologi and Geofisika (BMKG) at Soekarno-Hatta International Airport (CGK) were acquired via the University of Wyoming weather website (<https://weather.uwyo.edu/upperair/sounding.html>). Sounding data were available only at 0000 and 1200 UTC (0700 and 1900 LT, respectively), and only mandatory levels were retrieved. A climatological rainfall dataset (Global Precipitation Measurement [GPM] IMERG Level 3) was obtained (Huffman et al., 2019). This dataset has a 0.1° spatial resolution and 30-min time interval. A global 3-h, 0.25° -resolution sea surface temperature (SST) dataset was acquired from the Woods Hole Oceanographic Institution (WHOI) Climate Data Record (CDR) (Clayson et al., 2016). Finally, boundary-layer height estimates were retrieved from the ERA5 reanalysis dataset, which has a spatial resolution of 0.3° and temporal resolution of 1 h (Hersbach et al., 2020).

TABLE 2 Instruments specification.

Instruments	Brand and type [data logger]	Resolution	Accuracy/uncertainty	Sampling frequency (interval)	Parameters obtained
Ultrasonic anemometer	Gill Windmaster [Graphtec GL840 analog data logger]	Wind speed: $0.01 \text{ m} \cdot \text{s}^{-1}$ Sonic temperature: 0.01°C	Wind speed accuracy: $<1.5\% \text{ RMS @ } 12 \text{ m} \cdot \text{s}^{-1}$ Sonic temperature accuracy: $\pm 2^\circ \text{C}$ [between -20°C and $+30^\circ \text{C}$]	10 Hz (0.1 s)	U, V, W, T_s
Temperature humidity gauge	Vaisala HMP 155 with fan-aspirated radiation shield [Graphtec GL840 analog data logger]	Temperature: 0.0035°C (*) relative humidity (RH): $0.0025\% (*)$ (*) based on datalogger's analog to digital converter (ADC) resolution	Temperature accuracy: $\pm 0.055 + 0.0057 \times T^\circ \text{C}$ [between $+20^\circ \text{C}$ and $+60^\circ \text{C}$] RH accuracy: $\pm 1.0 + 0.008 \times \text{RH} \%$ [between -20°C and $+40^\circ \text{C}$]	10 Hz (0.1 s)	T, RH
Net radiometer	Kipp & Zonen CNR4 [Campbell Scientific CR1000]	Pyranometer: $<0.06 \text{ W} \cdot \text{m}^{-2}$ pyrgeometer: $<0.12 \text{ W} \cdot \text{m}^{-2}$	Pyranometer uncertainty: $<5\%$ (for daily total) pyrgeometer uncertainty: $<10\%$ (for daily total)	0.016 Hz (1 min)	R_s , L_d , L_u
Automatic weather station	Meter atmos 41 [Meter EM60G]	Rain gauge: 0.017 mm	Rain: $\pm 5\%$ of measurement	0.083 Hz (5 min)	Rain rate

4 | RESULTS

A monthly–diurnal composite of zonal wind speed (U) observed at the KKP and LLH buildings showed strong annual variation, shifting between positive (westerly) and negative (easterly) every year, with the direction remaining consistent at the diurnal scale (Figure 2a, b). The zonal wind component was dominated by easterlies from May to September, and by westerlies from December to March. During seasonal transition periods, zonal wind tended to be weaker and daily wind directions became less consistent. Sounding observations at CGK confirmed this shift (Figure 2c, d). Sounding data also indicated diurnal zonal wind consistency in the morning (0700 LT) and evening (1900 LT). Similar patterns were observed in both lower-level (1000 hPa) and upper-level (850 hPa) sounding, indicating consistent zonal wind directions throughout the boundary layer height (H_{bl}). Sounding data indicated the magnitude of observed near-surface zonal winds were consistent with lower-level sounding. However, higher-level sounding was seen at higher magnitudes, following the logarithmic boundary-layer wind profile (Arya, 2001; Stull, 1988).

Although they were dominated by annual signals, near-surface zonal winds observed at the KKP and LLH buildings also exhibited diurnal variation. Zonal wind magnitudes were stronger during the daytime

and weaker at night, consistent with the diurnal variation of near-surface wind speed observed by other researchers (e.g., Crawford & Hudson, 1973; Fajber et al., 2014; Jiménez et al., 2016). Stronger daytime near-surface winds were caused by rapid, efficient momentum transfer from aloft by the convectively unstable boundary layer, whereas the more stable night-time boundary layer will reduced downward momentum transport, hence resulting in slower near-surface winds (Arya, 2001; Fajber et al., 2014; Jiménez et al., 2016). The diurnal change in boundary layer stability condition is confirmed from stability parameter (ζ). The average value of ζ on both sites during daytime is ranged from -1 to -12.34 , indicating a very-unstable to extremely-unstable condition (Cantero et al., 2022; Sorbján & Grachev, 2010). Meanwhile during night-time, average ζ is ranged from -0.2 to 5.3 , indicating a weakly-unstable to extremely-stable condition.

By contrast, the meridional wind component (\bar{v}) exhibited a strong diurnal cycle (Figure 2e, f). Diurnal shifts between positive (southerly) and negative (northerly) values of V occurred throughout the observation period, indicating sea and land breeze circulation, respectively. Compared to KKP, southerly to northerly shifts at the LLH building occurred later, and the periods of northerly (sea breeze) winds were shorter, strongly suggesting that the sea breeze propagates from north (KKP)

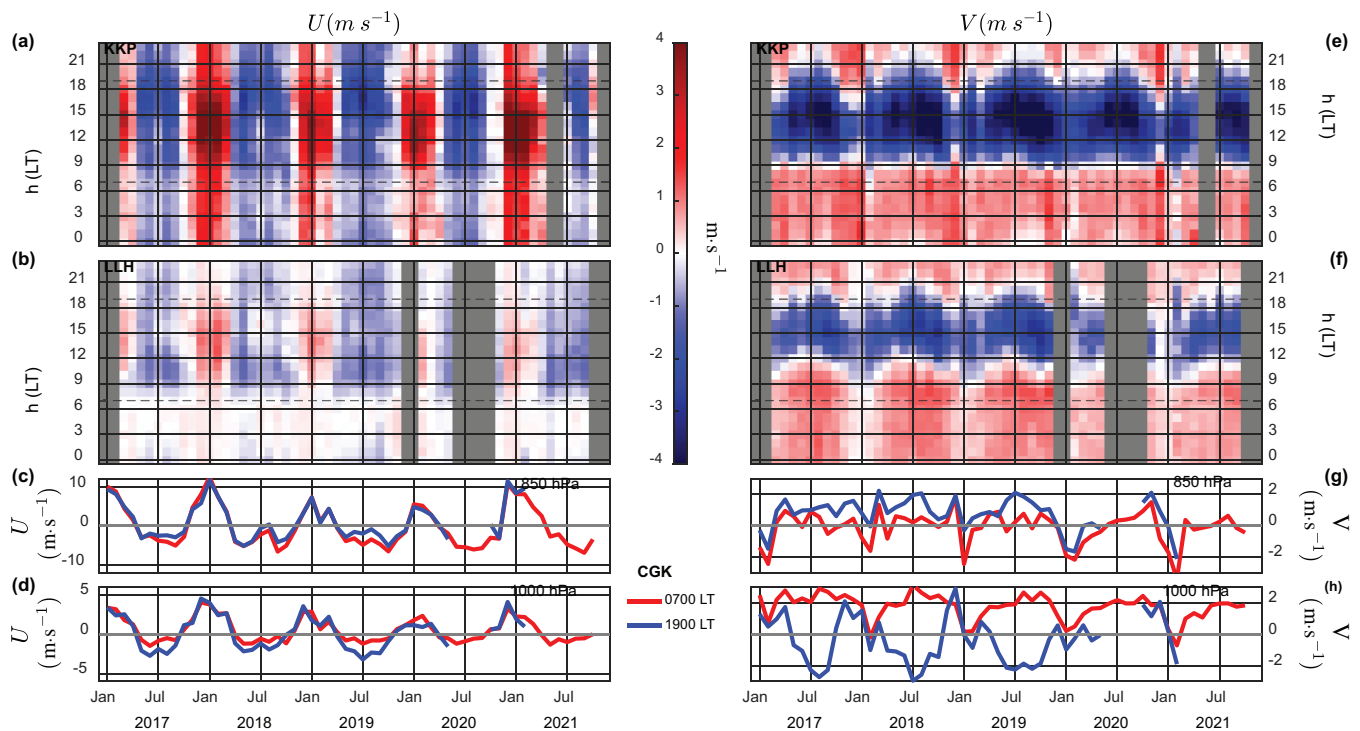


FIGURE 2 Monthly diurnal composite of zonal (U) and meridional (V) wind speed data observed at the (a, e) KKP and (b, f) LLH sites, compared to monthly averaged U and V data from sounding observations at CGK for (c and g) 850 hPa and (d and h) 1000 hPa. In (a, b, e, and f), horizontal dashed lines indicate the sounding measurements time, while block shading indicates missing data. [Colour figure can be viewed at [wileyonlinelibrary.com](https://onlinelibrary.wiley.com)]

to south (LLH). Sounding observations also provide evidence of these circulation patterns (Figure 2g,h). Meridional wind sounding at 0700 LT showed dominant southerly winds at the lower level (1000 hPa), with weak winds at the upper level (850 hPa), indicating a shallow land breeze. Conversely, sounding observations at 1900 LT indicated dominant northerly winds at the lower level and southerlies at the upper level, clearly indicating the sea breeze and its return flow aloft (anti-sea breeze), as also described in previous studies (Araki et al., 2006; Hadi et al., 2000; Hadi et al., 2002). Sounding data from December to February do not appear to show similar sea breeze circulation patterns, likely due to the shorter sea breeze duration (Figure 2e).

Because Jakarta is situated on the northern side of Java Island, wind decomposition into its zonal and meridional components can be used to separate annual and diurnal circulation patterns. The zonal wind can be used to identify seasonal changes, and meridional wind to identify the sea breeze.

4.1 | Zonal wind variation and seasonal change

Over the MC, seasons are typically categorized as dry or rainy according to the rainfall pattern (Chang, Wang,

et al., 2005b; Hamada et al., 2002; Tanaka, 1994). Transitions between the dry and rainy seasons are mainly driven by the monsoon regime change between the Asian winter (Australian summer) monsoon and Asian summer (Australian winter) monsoon (Belgaman et al., 2017; Chang, Wang, et al., 2005b). Within the Southern Hemisphere MC, including Jakarta, the Asian winter monsoon carries considerably more moisture from the eastern Indian Ocean and northern MC, mainly the South China Sea (Suwarman et al., 2013), thus, inducing more rainfall over this area. Conversely, the Asian summer monsoon carries less moisture and produces less rainfall. Thus, the Asian winter monsoon regime is regarded as the rainy season, and the Asian summer monsoon as the dry season.

Because the dry and rainy seasons are mainly defined in terms of rainfall, they vary among geographic locations, even within relatively short distances (Chang, Wang, et al., 2005b; Ferijal et al., 2022; Hamada et al., 2002; Moron et al., 2009). Based on pentad (5-day) rainfall variation, Jakarta's climatology has been classified as A–I, which is dominated by an annual cycle and a rainy season from September to February (Hamada et al., 2002). However, when using this classification system, rainy season length varies among stations in Jakarta. For example, at coastal stations such as Tanjung

Priok, the rainy season typically persists for 3 months (December–March), whereas at Halim, an inland station roughly 17 km from Tanjung Priok, the rainy season lasts for 5 months (November–April). To study the sea breeze, which can extend up to 80 km inland, a more robust definition of seasonal length is required. Therefore, in this study, we defined seasonal changes based on zonal wind patterns.

In this study, we used the strong annual variation exhibited by zonal winds as a parameter to determine the lengths of seasonal periods in Jakarta. A diurnal time series of monthly averaged U observed at both sites shows clear seasonal separation (Figure 3a,b). A diurnal pattern characterized by dominant easterlies was observed from May to September, whereas the opposite pattern was observed from December to March. The transition periods, that is, April, October, and November, are clearly distinguished by low winds throughout the day. By clustering these diurnal U patterns, we separated the seasons in Jakarta into a dry season from May to September and rainy season from December to March. Although this seasonal separation was based on wind data, we retain the terms “dry” and “rainy” because they are typically used to

distinguish seasons in this region. In this study, the transition from the rainy to dry season in April is referred to as transition 1 (tr1), and that from the rainy to dry season in October or November is referred to as transition 2 (tr2).

The atmospheric conditions for several seasonal periods are shown in Figure 3c–f. The maximum daily total net radiation energy (R_N) occurred during the late dry season (September), with a second peak in April (Figure 3c). Minimum R_N values were observed in January during the rainy season and June during the dry season. The maximum and minimum R_N values appeared to follow the equinox and solstice, respectively. Annual daily mean T showed a similar pattern to R_N , but with a clear lag (Figure 3d). Peaks of T were observed in May (dry season) and October (tr2), whereas the minimum T values were observed in late January and July, following a net radiation minimum in June. Although the net radiation minima were similar in magnitude, minimum T values during the rainy season were much lower than in the dry season. This suggests that another T regulatory mechanism, such as cold air advection, may dominate during the rainy season (Chang, Harr, & Chen, 2005). In tropical Jakarta, high RH values of >60% were

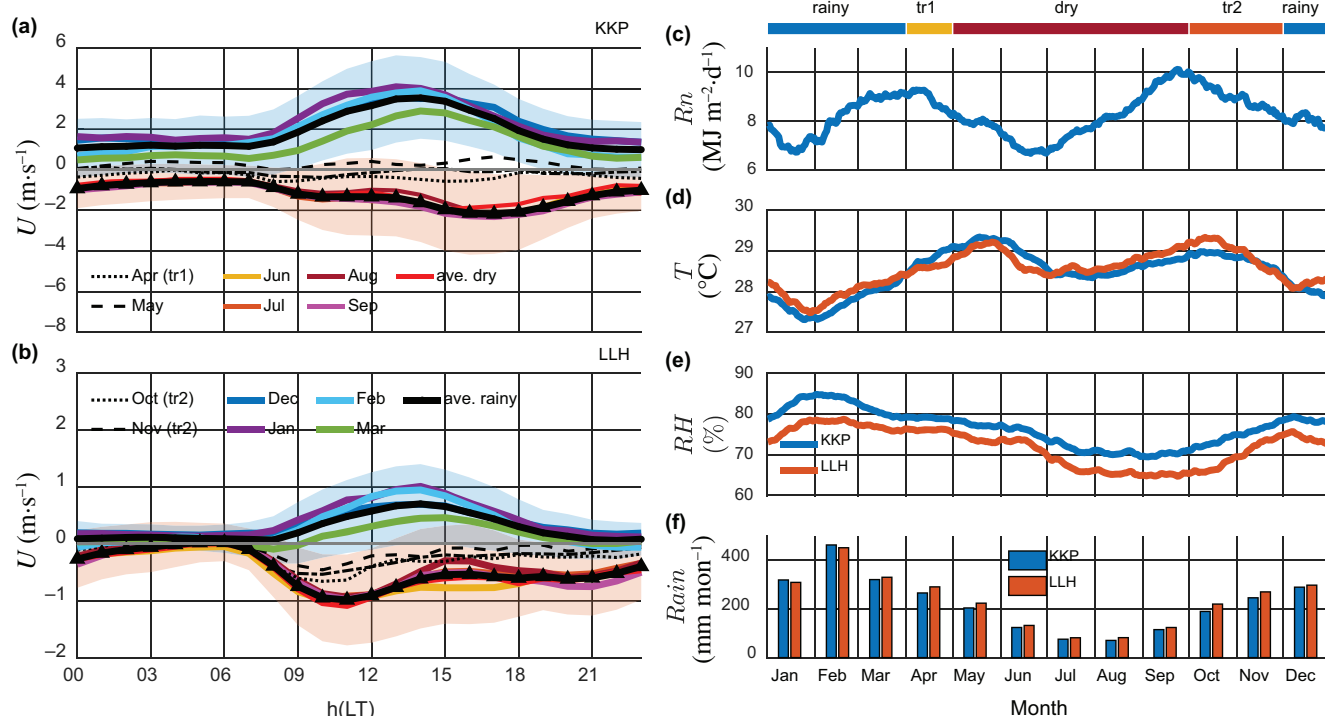


FIGURE 3 (Left) Diurnal time series of monthly averaged zonal wind speed (U) observed at the (a) KKP and (b) LLH sites. Lines with triangles and circles indicate the mean value of U during dry and rainy period, respectively. The shaded areas are the standard deviation from the mean values. (Right) Multiyear (c) mean daily total net radiation, (d) daily average temperature, and (e) relative humidity measured at the KKP and LLH sites, and (f) monthly accumulated rainfall obtained from the Global Precipitation Measurement (GPM) dataset. For image clarity, data were smoothed using a 31-day moving average filter. GPM data were averaged around each site using a 9-point average. Seasonal periods based on zonal wind are indicated at the top of the right panel. [Colour figure can be viewed at wileyonlinelibrary.com]

observed throughout the year (Figure 3e). The lowest RH values occurred in the last 3 months of the dry season (July–September), whereas the maxima occurred at the peak of the rainy season, from late January to early February. Maximum and minimum rainfall amounts were observed in February and July–September, respectively. Applying the wind-based seasonal period thresholds to the GPM rainfall data, we found that the monthly rainfall in Jakarta was $<200 \text{ mm} \cdot \text{month}^{-1}$ during the dry season and $>300 \text{ mm} \cdot \text{month}^{-1}$ during the rainy season.

4.2 | Meridional wind variation and sea breeze identification

The seasonal mean meridional wind data shown in Figure 4a,b suggest that sea breeze circulation was dominant in both seasons. A northerly to southerly shift before noon and southerly to northerly shift after sunset were clearly observed at both sites. Hadi et al. (2002) argued that daytime enhancement of low-level northerlies during the rainy season was unlikely to have been caused by the sea breeze due to a lack of obvious land–sea temperature differences and subdued seaward return flow. However, a comparison of T at KKP and sea surface temperature (SST) near Jakarta (Figure 4c) showed that daytime land–sea temperature differences occurred in both seasons. While over land T shows

significant variation between dry and rainy season, SST during both seasons does not differ significantly; thus, seasonal sea breeze variation in Jakarta might be primarily affected by temperature dynamics over land rather than over the sea.

The diurnal variation in peak northerly wind between seasons is shown in Figure 4a,b. The peak magnitude of northerly wind differed significantly between the dry and rainy seasons; whereas that during the dry season was nearly double that in the rainy season. We also observed seasonal variation in the time of peak northerly wind, which occurred at approximately 1300 LT in the rainy season and approximately 1500 LT in the dry season at KKP. A similar transition was observed at LLH, but with a 1-h lag. These findings are in contrast with those of a previous study showing that the timing of the peak northerly anomaly did not vary seasonally (Araki et al., 2006).

Another striking feature revealed by comparing Figure 4a,b with Figure 2e,f is a clear discrepancy in the southerly to northerly shift between KKP and LLH. This shift occurred at approximately 0900 LT at KKP, whereas its timing varied seasonally at LLH. At LLH, the shift occurred earlier in the rainy season than the dry season, suggesting seasonal variation in the V_{SBF} . The positioning of the KKP and LLH sites allowed us to estimate this parameter using the intrusion time and distance between sites.

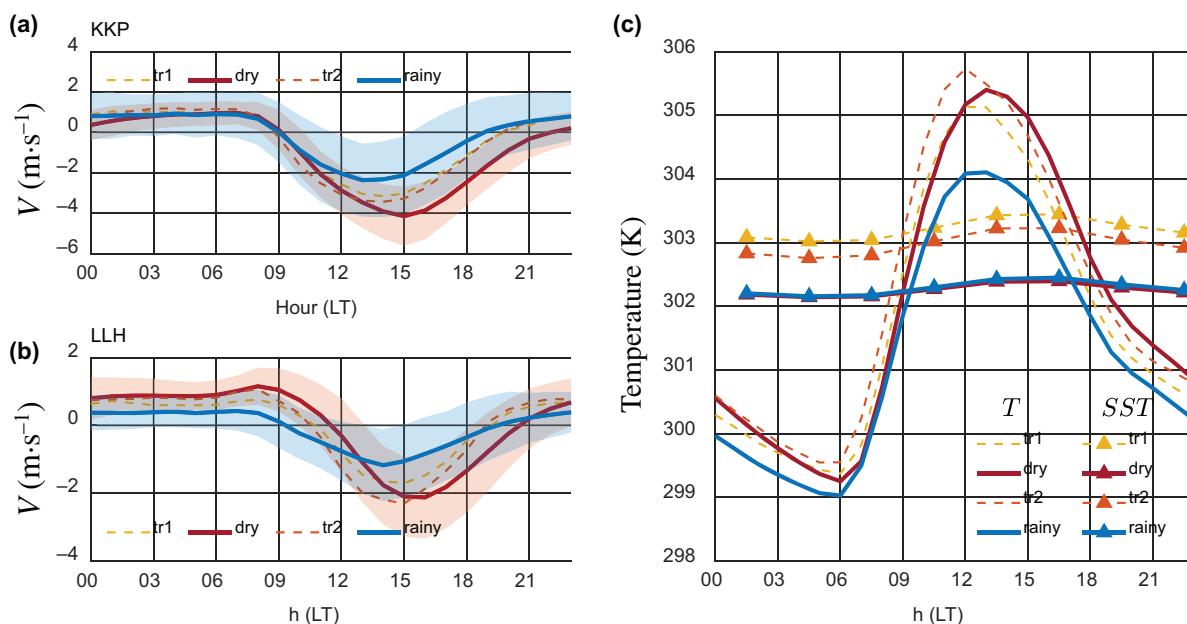


FIGURE 4 Seasonal average hourly meridional wind speed (V) observed at the (a) KKP and (b) LLH sites, and seasonal average air temperature (T) at KKP and sea surface temperature (SST) on the Java Sea, north of Jakarta. Shadings in (a, b) were standard deviations of V from its average values. [Colour figure can be viewed at [wileyonlinelibrary.com](https://onlinelibrary.wiley.com/doi/10.1002/joc.8139)]

To further investigate sea breeze seasonal variation, we constructed a dataset of selected sea breeze occurrences or sea breeze days. Sea breezes were identified based on front intrusions at each site. Front intrusion onset was indicated by a sharp change in wind direction, accompanied by a rapid increase in humidity. Similar methods have been used in several previous studies (e.g., Ferdiansyah et al., 2020; Hadi et al., 2002; Jayakrishnan et al., 2021; Reddy et al., 2021). Because the Jakarta coastline runs in the east–west direction, we assumed that the sea breeze mainly blows from north (sea) to south (land). We used positive to negative shifts in the meridional wind component (V) to identify the onset of sea breeze intrusion, and the opposite shift to identify sea breeze cessation. We further refine the identification process by using the abrupt increase in humidity to clear-cut when the intrusion time of sea breeze occurs and discard doubtful cases where the wind shift might be caused by other phenomena (Sumner, 1977).

We calculated a daily 10-min average time series of the observation data to obtain a clearer understanding of the timing of sea breeze intrusion and cessation. Because significant temperature drops were not typically observed during sea breeze intrusion in Jakarta, we used only V , wind direction, and RH for sea breeze identification. A representative daily time series of these factors for 5 August, 2018 are shown in Figure 5, where sea breeze intrusion occurred at approximately 1030 LT (1230 LT) at KKP (LLH) and sea breeze cessation occurred at approximately 20:10 LT (2020 LT) at LLH (KKP). These thresholds were identified using a semi-automatic process for all available data; we applied a simple change detection algorithm followed by manual correction.

For V_{SBF} estimation, intrusion times for both sites were required; therefore, only days satisfying this requirement were retained in the dataset. Days with sea breeze intrusion detected at both sites were retained as sea breeze days; all other days were considered non-sea breeze days. For each sea breeze day, the cessation time at both sites was also identified. The cessation time of sea breeze is also regarded as the intrusion time of land breeze at each site. The sea breeze cessation time was identified only from V shifts because most data showed no obvious humidity changes during these periods. This might have reduced the accuracy of cessation time estimations; however, as most of the data indicate sharp wind direction shifts, as shown in Figure 5b, we considered the results valid.

We identified 810 sea breeze days from among 1121 days with available data throughout the observation period. The percentages of sea breeze and non-sea breeze days are shown in Figure 6. Most sea breeze days occurred between March and November, consistent with

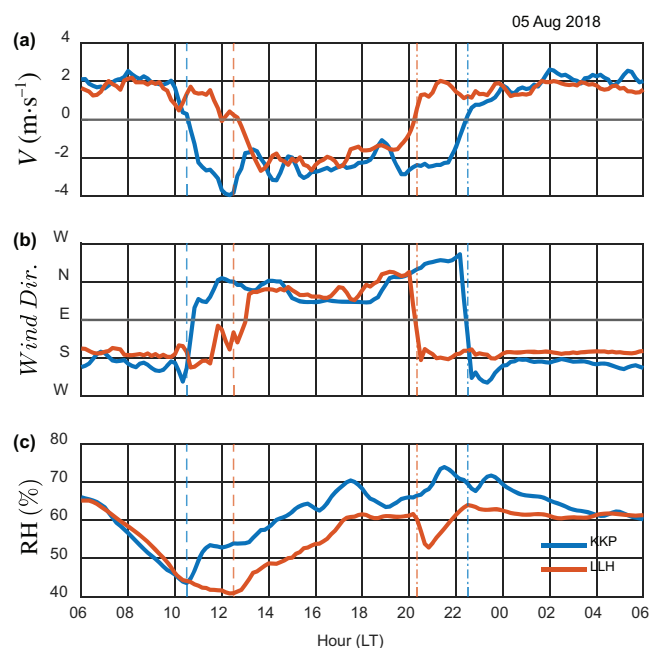


FIGURE 5 Example of 10-min averaged (a) meridional wind speed (V), (b) wind direction (D), and (c) relative humidity (RH) observed at the KKP and LLH sites on August 5, 2018. Plots are smoothed using a 30-min moving average window. Vertical dashed and dashed-dot lines indicate the sea breeze intrusion and cessation time, respectively. [Colour figure can be viewed at [wileyonlinelibrary.com](https://onlinelibrary.wiley.com/doi/10.1002/joc.8139)]

the findings of previous studies (Araki et al., 2006; Hadi et al., 2002). Fewer sea breeze days were identified during December, January, and February. Araki et al. (2006) found that the sea breeze signal was less clear, but nevertheless distinguishable, during this period, especially on days with weak prevailing winds. Data were unavailable for many days during this period due to rainfall screening; thus, the number of sea breeze days was underestimated.

4.3 | Seasonal variation in sea breeze

The monthly distribution of sea breeze intrusion times at both sites in Jakarta is shown in Figure 7a. At KKP, sea breezes arrived earlier in the rainy season, and at tr_2 , than in the dry season and at tr_1 . If the sea breeze intrusion at KKP represents the sea breeze onset at Jakarta, then the sea breeze occurs faster in the rainy than dry season, although the earliest occurrence was in October (tr_2). The interquartile range of sea breeze intrusion time shows fluctuation of approximately 0.5–1 h around the median value. The seasonal average intrusion time is provided in Table 3, and indicates an approximately 30-min difference in sea breeze onset between the rainy and dry

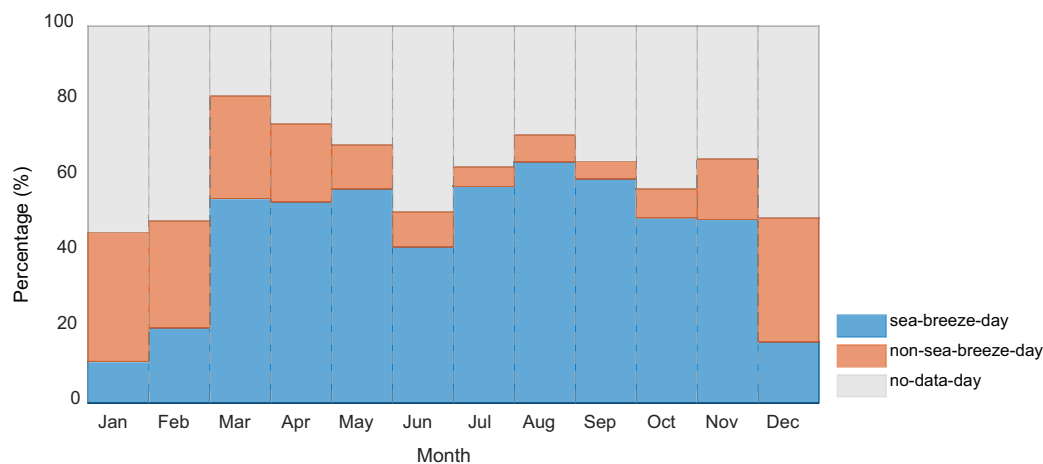


FIGURE 6 Monthly percentages of sea breeze days, non-sea breeze days, and days with no data from January 2017 to December 2021. [Colour figure can be viewed at wileyonlinelibrary.com]

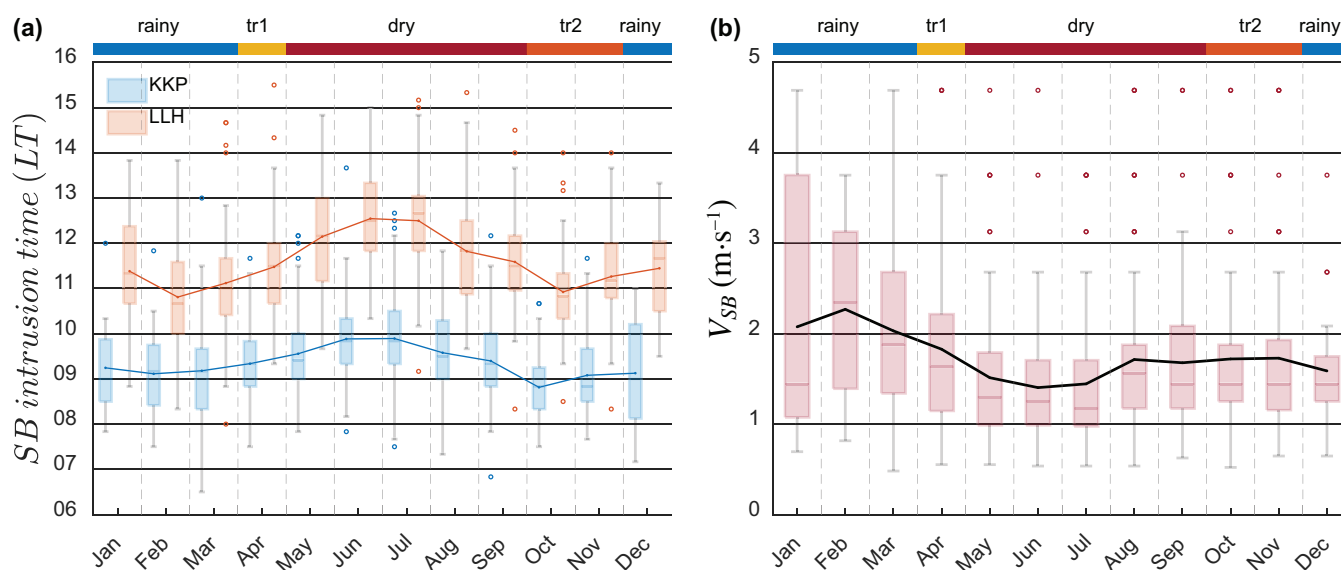


FIGURE 7 (a) Boxplot of sea breeze intrusion times at Kementrian Kelautan dan Perikanan (KKP) and Laboratorium Lingkungan Hidup (LLH) and (b) sea breeze propagation speed (V_{SBF}). Dotted lines represent mean values for each month. Seasonal periods are indicated at the top of each plot. [Colour figure can be viewed at wileyonlinelibrary.com]

seasons. This difference impacts sea breeze intrusion at LLH, where it arrives later during the dry season.

Table 3 also shows the seasonal averages of sea breeze cessation time and duration. In this study, sea breeze duration was defined as the time difference between sea breeze cessation and intrusion at KKP, which was found to vary seasonally. At KKP, the cessation time was typically 1900–1930 LT, except in the dry season, when the sea breeze started late, but lasted until 21:00, that is, for a longer duration (>11 h) than in the rainy season (<10 h).

The late sea breeze arrival at LLH during the dry season was caused by both late-onset and lower propagation speed. The slowest sea breeze propagation was observed from May to July, and the fastest was in February (Figure 7b). During

the dry season, the average V_{SBF} was approximately $1.56 m \cdot s^{-1}$, similar to previous observations based on satellite-derived cloud lines (Ferdiansyah et al., 2020). V_{SBF} was $0.55 m \cdot s^{-1}$ slower in the dry than rainy season (Table 3). The interquartile range of V_{SBF} also suggested that V_{SBF} tended to be higher during the rainy season.

5 | DISCUSSION

5.1 | Sea breeze onset

Based on Equation (1), sea breeze onset depends on the rate at which positive ΔT between land and sea develops.

TABLE 3 Seasonal averages of sea breeze characteristics observed in Jakarta.

Characteristic		tr1	Dry	tr2	Rainy
Average (Avg.) intrusion time (LT)	KKP	9:20	9:40	9:00	9:10
	LLH	11:30	12:10	11:10	11:10
Avg. cessation time (LT)	KKP	19:30	21:00	19:30	19:00
	LLH	18:50	19:30	18:20	17:40
Avg. duration (h)		10.18 ± 2.2	11.30 ± 2.7	10.50 ± 2.6	9.80 ± 3.0
Avg. propagation speed (m · s ⁻¹)		1.83 ± 0.9	1.56 ± 0.8	1.72 ± 0.8	2.01 ± 1.0

Abbreviations: LLH, Laboratorium Lingkungan Hidup; KKP, Kementerian Kelautan dan Perikanan.

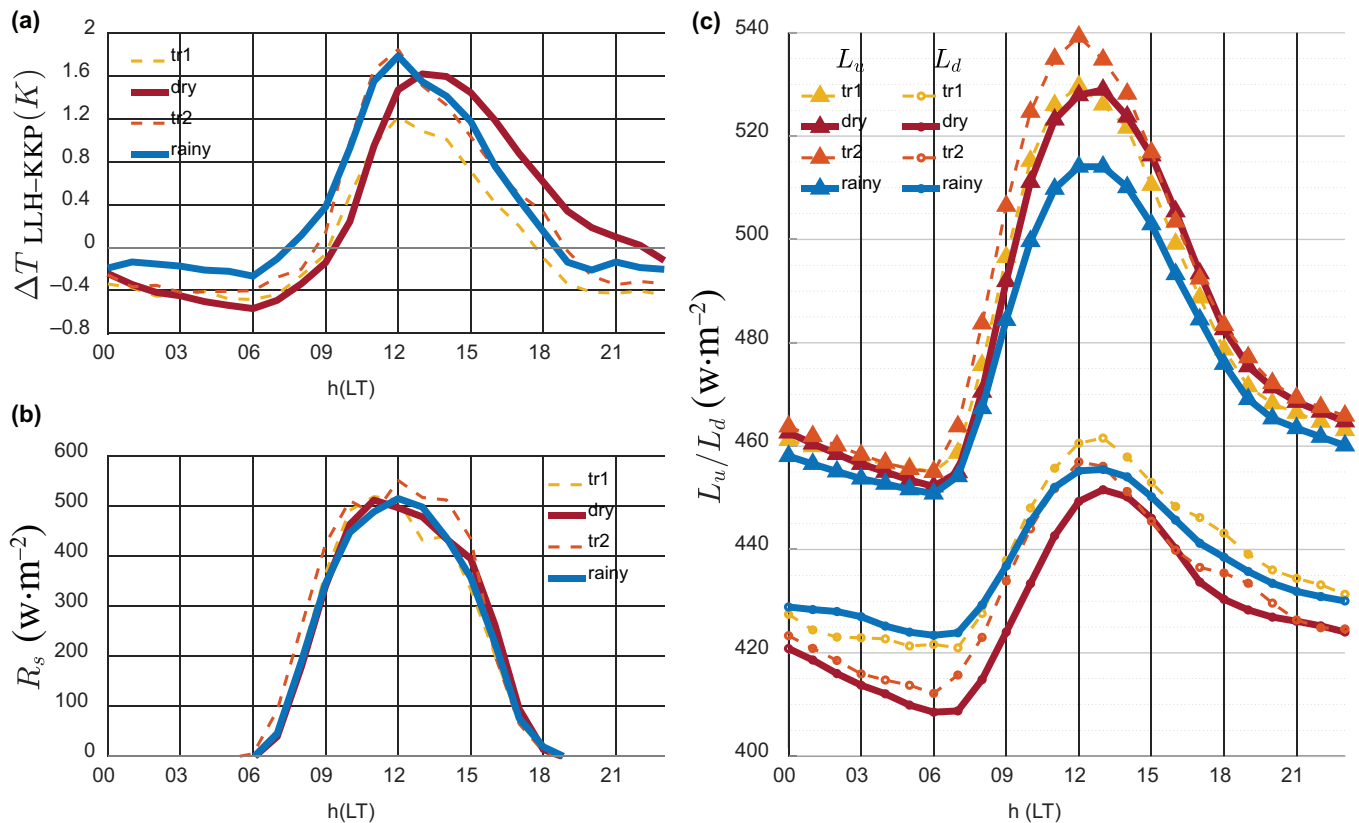


FIGURE 8 (a) Seasonal average hourly temperature differences between observations taken at Laboratorium Lingkungan Hidup (LLH) and Kementerian Kelautan dan Perikanan (KKP) ($\Delta T_{LLH-KKP}$). (b) Net shortwave radiation (R_s) and (c) upward and downward components of longwave radiation (L_u and L_d) at LLH. [Colour figure can be viewed at [wileyonlinelibrary.com](https://onlinelibrary.wiley.com/terms-and-conditions)]

Earlier sea breeze onset during the rainy season is likely caused by an earlier shift of ΔT , as clearly shown by the temperature difference between LLH and KKP ($\Delta T_{LLH-KKP}$) (Figure 8a). The change from negative to positive ΔT occurred at approximately 0730 LT in the rainy season but at approximately 0930 LT in the dry season. A previous model simulation showed that sea breeze onset is sensitive to prior surface energy conditions (Junnaedhi et al., 2021); thus, seasonal sea breeze variation can be explained using a surface energy budget. According to Oke et al. (2017), the surface energy budget over an urban area volume is defined as follows:

$$R_N + Q_F = Q_H + Q_L + \Delta Q_S + \Delta Q_A, \quad (7)$$

where Q_H and Q_L are the sensible and latent heat flux, respectively, to or from the air, ΔQ_S is the change in above-ground energy storage within the urban volume, which represents the heat capacity of all canopy elements, and ΔQ_A is the net energy added to or subtracted from the volume by advection. On the left-hand side of Equation (7), Q_F is the anthropogenic heat flux, which is the heat released within the volume by human activities, and R_N is the net radiation at the surface, which is the sum of net shortwave (R_S) and net longwave (R_L) radiation, calculated as follows:

$$R_N = R_S + R_L = S_d - S_u + L_d - L_u, \quad (8)$$

where S and L are shortwave and longwave radiation, respectively, and subscripts u and d are the upward and downward radiation components, respectively.

In the morning, prior to sea breeze onset, R_S observations in Jakarta showed no significant difference between the dry and rainy seasons (Figure 8b). Assuming little seasonal variation in anthropogenic heat production at this hour, discrepancies in $\Delta T_{LLH-KKP}$ may be attributed to variation in R_L . Downward longwave radiation (L_d) was higher in the rainy than dry season, whereas upward longwave radiation (L_u) showed slight variation between seasons (Figure 8c). This indicates that downward influx was more prominent than lower surface cooling prior to sea breeze onset. Downward radiative longwave influx, that is downwelling, is mainly derived from clouds (Arya, 2001), which may form in the afternoon and move offshore via the land breeze (Mori et al., 2018), or may develop close to shore due to land breeze and monsoon convergence (Wu et al., 2007). Early morning cross-shore clouds that scatter across the city can reduce temperature differences by distributing heat between the coast and inland areas, which induces a positive ΔT more rapidly when shortwave radiation (R_s) is available, ultimately causing earlier sea breeze onset.

By contrast, post-midnight ΔT values were more negative during the dry than rainy season (Figure 8a). More negative ΔT values indicate inhomogeneous cooling rates between coastal and inland areas. Between 0000 and 0600 LST, the average temperature dropped by 1.2 and 1.5 K at KKP and LLH, respectively. Dryer surfaces cause more intense radiative cooling during the night over inland areas, whereas coastal areas are warmer due to the proximity to the sea. If few or no clouds are available to distribute heat, strong negative cross-shore temperature differences occur before sunrise, such that more time is required for a similar amount of R_s (Figure 8b) to overcome negative ΔT , thus delaying sea breeze onset.

5.2 | Sea breeze propagation speed

Seasonal variation in V_{SBF} peaked during the rainy season (February) and reached a minimum in the dry season (June) (Figure 7b). To assess seasonal variation in V_{SBF} , we used Equation (3) to estimate V_{SBF} from $\Delta T_{LLH-KKP}$ using V measured at LLH as V_g , and estimated d using the H_{bl} from the ERA5 dataset. Then, V_{SBF} was estimated 30 min after sea breeze intrusion at KKP, under the assumption that temperature at KKP during this time can be used to represent sea breeze gravity current

temperature and the front was still located between KKP and LLH. These estimated V_{SBF} values were termed $V_{SBF(est)}$, and those obtained from detected meridional wind and humidity changes were termed $V_{SBF(obs)}$.

Direct comparison of $V_{SBF(est)}$ and $V_{SBF(obs)}$ on a daily basis does not yield a clear relationship due to various factors not reflected in the V_{SBF} estimation, which assumes homogeneous density of both the sea breeze current and ambient air; however, density actually varies across the respective air masses. Another influential factor is the use of surface-level variables, which are prone to the effects of super adiabatic-layer and surface-layer turbulence (Reible et al., 1993). The magnitude of $V_{SBF(est)}$ is also sensitive to sea breeze depth (d). To match the magnitude of $V_{SBF(obs)}$, we determined an optimum d value of $0.75 H_{bl}$. Despite these, however, monthly composite of $V_{SBF(est)}$ and $V_{SBF(obs)}$ showed remarkably similar patterns (Figure 9), with higher propagation speed during the rainy season and lower speed during the dry season and transition periods. This demonstrates that Equation (3) is still applicable for estimating the V_{SBF} at monthly and seasonal time scales.

The separation of components in Equation (3) clearly confirms the dependence of V_{SBF} on the temperature difference (Figure 10a), as $\Delta T/T$ is clearly higher in the rainy season than during other periods, such that the V_d (first term) is also higher. This result corresponds well with the observed V_{SBF} values (Figures 7b and 9). In the dry season, $\Delta T/T$ was significantly lower; therefore, V_{SBF} was also lower. However, observed and estimated V_{SBF} also increased slightly in August and September, respectively, which was attributed to higher d (Figure 10b). Seasonal variation in d showed the opposite trend to $\Delta T/T$. As temperature is higher during the dry season (Figure 3d), H_{bl} was also higher; therefore, sea breeze depth was greater. Although seasonal variation in d varied significantly, it did not significantly affect the seasonal variation of $V_{SBF(est)}$. The seasonal pattern of $V_{SBF(est)}$ was still greatly affected by the temperature difference.

The opposing flow (V_g), that is the land breeze, was also driven by negative ΔT during the previous night. As shown in Figure 10c, the opposing flow was weaker in the rainy than dry season; thus, the SBF moved faster in the rainy season. In January and February, the opposing flow was negligible; thus, the V_{SBF} was equal to the V_d . Post-midnight heat distribution via cloud downwelling in the rainy season caused less negative ΔT and weakened the land breeze, whereas more negative ΔT in the dry season produced stronger opposing flow, which reduced the V_{SBF} . These findings confirm that overland temperature difference is the main factor governing sea breeze seasonality in Jakarta.

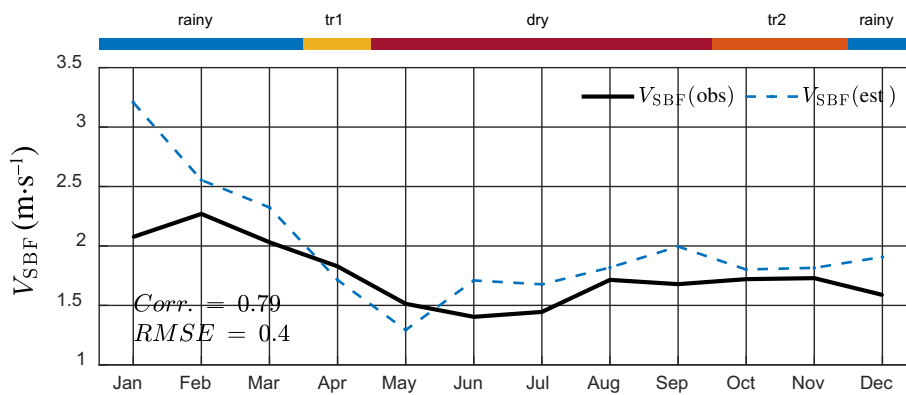


FIGURE 9 Monthly composite of observed ($V_{\text{SBF}(\text{obs})}$) and estimated ($V_{\text{SBF}(\text{est})}$) sea breeze front propagation speed. [Colour figure can be viewed at [wileyonlinelibrary.com](https://onlinelibrary.wiley.com/doi/10.1002/joc.8139)]

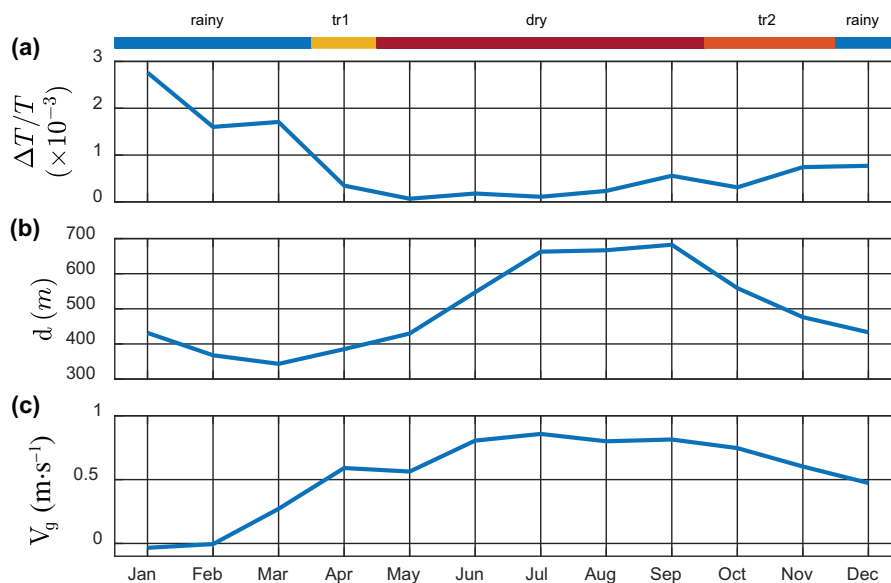


FIGURE 10 Monthly composite of (a) normalized temperature difference ($\Delta T/T$), (b) sea breeze depth (d), and (c) opposing flow (V_g), which were used to calculate $V_{\text{SBF}(\text{est})}$ according to Equation (3). [Colour figure can be viewed at [wileyonlinelibrary.com](https://onlinelibrary.wiley.com/doi/10.1002/joc.8139)]

5.3 | Sea breeze duration

Longer sea breeze duration in the dry season was caused by prolonged positive ΔT during the night (Figure 8a). After dawn, positive ΔT was maintained by higher sensible heat release in the urban core area compared to the coast (Figure 11a,b). At KKP, Q_H dropped rapidly below $20 \text{ W} \cdot \text{m}^{-1}$ after 1800 LT, whereas at LLH, Q_H remained higher than at KKP until 2200 LT. This discrepancy maintained the temperature differences between the urban core and coast, which ultimately prolonged sea breeze flow. In the rainy season, Q_H at both sites dropped to a similar value around sunset, such that positive ΔT was no longer sustained and the sea breeze flow ceased.

In the absence of incoming R_s , night-time heat release is mainly derived from the energy storage (ΔQ_s) term in Equation (7). In the dry season, longer sensible heat release in LLH was caused by the higher thermal inertia of urban surfaces, due to the urban volume could store more energy during the daytime and release it over a longer period during the night (Grimmond & Oke, 1999; Oke et al., 2017). Conversely, coastal Jakarta has less thermal inertia, as it mainly comprises residential and recreational areas, whereas the

larger vegetated areas and proximity to the sea significantly suppress the night-time Q_H release in preference for Q_L release. Thus, night-time sensible heat (Q_H) release over coastal Jakarta did not differ significantly among seasons (Figure 11a), demonstrating that urban areas can alter sea breeze duration, particularly during the dry season. During the rainy season, rainfall, which usually occurs from afternoon until midnight (Renggono et al., 2001), wets urban surfaces such that Q_L release is preferable to Q_H release. Thus, night-time Q_H release over the urban area is reduced and positive ΔT values are dispersed, such that the sea breeze effectively ceases at earlier time. This seasonal discrepancy in duration may indicate significant effect of urban area of Jakarta to the seasonality of sea breeze.

5.4 | Influence of urban area to seasonal sea breeze variation

While V_{SBF} estimation using Equation (3) confirm that temperature difference overland and strength of opposing flow are the main factor in sea breeze seasonality, it did not consider many realistic physical settings and urban

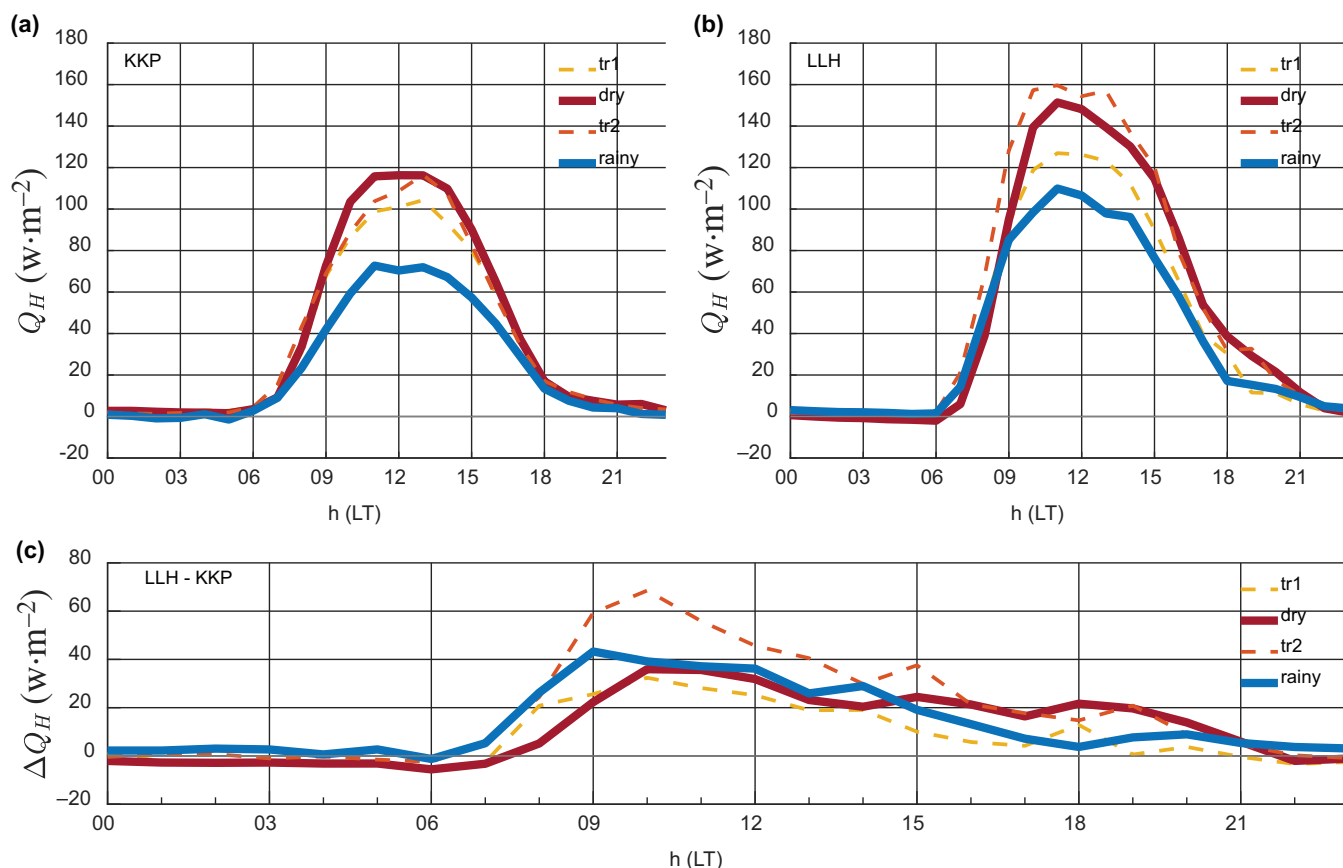


FIGURE 11 Seasonal average of hourly sensible heat flux (Q_H) observed at (a) Kementrian Kelautan dan Perikanan (KKP) and (b) Laboratorium Lingkungan Hidup (LLH), and (c) seasonal Q_H difference between LLH and KKP. [Colour figure can be viewed at [wileyonlinelibrary.com](https://onlinelibrary.wiley.com/doi/10.1002/joc.8139)]

properties that influence sea breeze, such as topography, coastal orientation, surface friction, surface heating and UHI circulation. Exclusion of such factors is causing the $V_{\text{SBF}(\text{est})}$ to tend to be overestimate the $V_{\text{SBF}(\text{obs})}$. Among the aforementioned factors, topography and coastal orientation might not have a significant effect to sea breeze propagation over Jakarta. Averaged topographical slope of Jakarta is less than $1.9 \text{ m} \cdot \text{km}^{-1}$ in the inland direction (Badan Informasi Geospasial, 2018), thus can be considered almost flat. Along Jakarta Bay's coast, sea-breeze-associated-cloud-line was observed moving in similar speed, at least before reaching city centre (Ferdiansyah et al., 2020). On the other hand, surface friction induced by urban roughness elements, such as buildings, structures, and trees, may have more effect on V_{SBF} . Using building-resolving computational fluid dynamics (CFD) simulation with plan area density (λ_p) 0.25, Jiang et al. (2017) showed that increasing average buildings height by 40 m could reduce V_{SBF} by 16%. The average building height in Jakarta is between 5 and 20 m, and the averaged λ_p is 0.2 (Darmanto et al., 2017), thus, we expect the reduction of V_{SBF} due to urban roughness will be less than 16%. This reduction, however, may not contribute to seasonal

variation of V_{SBF} as the urban roughness element can be assumed constant throughout the year.

Instead of roughness, surface heating variation may have more effect on seasonal variation of sea breeze propagation in Jakarta. V_{SBF} estimation in Equation (3) assumes sea breeze gravity current move with nearly constant internal temperature. In reality, as the sea breeze gravity current propagate inland, it was continuously heated at an increasing rate by the surface, creating an internal temperature gradient within the interior of the cold current. This gradient will induce internal vorticity, which strengthening surface wind speed. As the front side of the gravity current is heated at longer time, the temperature difference across the front is reduced, thus, effectively slowing the front propagation speed (Robinson et al., 2013). Daytime surface heating rate (represented by Q_H in Figure 11a,b) in dry season is higher than rainy season, with peak-to-peak difference up to $40 \text{ W} \cdot \text{m}^{-2}$. In the rainy season, Q_H release over the urban area is reduced significantly by rigorous Q_L release due to wet surface (Oke et al., 2017). Taking into account this surface heating difference, it is expected that in dry season V_{SBF} will be slower than in the rainy season. Observed surface sea breeze wind

speed (Figure 4a,b), which shows higher speed in the dry season than rainy season, also indicates the effect of continuous surface heating onto the sea breeze propagation speed.

Sea breeze onset and propagation speed variation may also be affected by daytime UHI circulation, which becomes significant since the width of Jakarta's urban area exceeds 10 km (Yoshikado, 1994). Existence of UHI circulation in the morning can accelerate sea breeze intrusion on land (Cenedese & Monti, 2003; Yoshikado, 1992). In the afternoon, when sea breeze front merges with the thermal upward flow of UHI circulation, which usually occurs at the urban core area, a larger and stronger front will develop. At the surface level, the merged upward flow will increase the wind speed, but at the same time it will create a thermal blockage to the advancing gravity current, hence reduce its propagation speed over urban core area (Varquez et al., 2015; Yoshikado, 1992).

To produce UHI circulation in relatively weak background winds, only a minimum of $20 \text{ W} \cdot \text{m}^{-2}$ excess of heat flux over urban core area is needed (Wang et al., 2019). Prior to sea breeze intrusion at the coastal area (KKP), which typically occurs around 0900 LT (Table 3), the sensible heat flux difference (ΔQ_H) between urban area and coastal area (LLH and KKP) could reach up to $40 \text{ W} \cdot \text{m}^{-2}$ in the rainy season, but only $20 \text{ W} \cdot \text{m}^{-2}$ in the dry season (Figure 11c). This observation suggests that a stronger morning UHI circulation may be developed in the rainy season that contribute to earlier sea breeze intrusion in Jakarta. Merge between sea breeze front and UHI upward flow might slow sea breeze propagation over Jakarta's urban core area. Previous studies showed that sea-breeze-associated-cloud-lines move faster in the west and east sides of Jakarta when reaching urban core area and stagnant clouds were observed over the city center (Ferdiansyah et al., 2020). In the estimation of V_{SBF} using Equation (3), we assumed that the UHI contribution is included in $\Delta T_{\text{LLH-KKP}}$. However, our current observation is not adequate to quantitatively assess the effect of UHI on V_{SBF} . To assess the effect of UHI, additional observations outside the urban area of Jakarta will be required to make the comparison with the existing urban observations. Such comparison could also be used to confirm the significant impact of urban area development and urbanization to sea breeze onset and duration. Furthermore, to account for previously discussed surface heating effect, the use of high-resolution numerical simulations with real physical setting will also be necessary.

6 | SUMMARY AND CONCLUSION

In this study, we analysed seasonal variation in the characteristics of the sea breeze in Jakarta using multi-year near-surface observation data for wind, temperature,

humidity, and radiation. Observations were conducted from March 2017 to October 2021 at two urban sites in Jakarta, namely KKP and LLH, which are located on the coast of Jakarta Bay and in the urban core, respectively, separated by a distance of approximately 11 km in the cross-shore direction, such that sea breeze propagation between them could be measured.

Decomposed wind observations showed a strong relationship between diurnal zonal wind and annual circulation, which we used to differentiate the dry (May–September) and rainy (December–March) seasons in Jakarta, separated by transition periods in April (tr1) and October–November (tr2).

Sea breeze onset, propagation speed, and duration showed strong seasonal variation. In Jakarta, the sea breeze started earlier, propagated faster, and was of shorter duration during the rainy than dry season. Seasonal variation in sea breeze onset and propagation speed was mainly driven by variation in temperature differences in the daytime or night-time prior to sea breeze occurrence. The presence of clouds during the night played an important role in terrestrial heat distribution, which governed sea breeze onset and propagation speed. Seasonal variation in urban surface heating and UHI circulation may also affect sea breeze onset and propagation speed over urban area of Jakarta. The Jakarta urban area also prolonged the sea breeze duration, especially during the dry season. Due to its larger thermal inertia, the urban core stored more energy during the day and released it more slowly overnight, thus prolonging positive temperature differences between urban and coastal areas and promoting longer sea breeze flow.

AUTHOR CONTRIBUTIONS


I Dewa Gede Agung Junnaedhi: Conceptualization; data curation; methodology; visualization; writing – original draft; writing – review and editing; formal analysis; validation. **Atsushi Inagaki:** Conceptualization; data curation; supervision; funding acquisition; methodology; project administration; software; writing – review and editing; validation; resources. **Muhammad Rezza Ferdiansyah:** Data curation; writing – review and editing; resources. **Manabu Kanda:** Conceptualization; supervision; funding acquisition; project administration; resources; writing – review and editing.

ACKNOWLEDGEMENTS

This research was funded by Japan Society for Promotional of Science (JSPS) KAKENHI grants (nos. 21H04573 and 19KK0105). The first author was funded by a scholarship from the Indonesian Endowment Fund (LPDP). The authors thank Mr. Nasir (KKP), Mr. Andi (LLH), and Mr. Tamrin (LLH) for their support with the observations. We also appreciate the comments and

suggestions from Mr. Alexandros Marios Makedonas and Mr. Do Ngoc Khanh for the first draft of the manuscript.

ORCID

I Dewa Gede Agung Junnaedhi  <https://orcid.org/0000-0003-0087-4405>

REFERENCES

- Araki, R., Yamanaka, M.D., Murata, F., Hashiguchi, H., Oku, Y., Sribimawati, T. et al. (2006) Seasonal and interannual variations of diurnal cycles of wind and cloud activity observed at Serpong, west Jawa, Indonesia. *Journal of the Meteorological Society of Japan. Ser. II*, 84A, 171–194. Available from: <https://doi.org/10.2151/jmsj.84A.171>
- Argüeso, D., Di Luca, A. & Evans, J.P. (2016) Precipitation over urban areas in the western maritime continent using a convection-permitting model. *Climate Dynamics*, 47(3), 1143–1159. Available from: <https://doi.org/10.1007/s00382-015-2893-6>
- Arya, P.S. (2001) *Introduction to micrometeorology*. San Diego, California, London, UK: Academic Press.
- Azarin-Molina, C., Chen, D., Tijm, S. & Baldi, M. (2011) A multi-year study of sea breezes in a Mediterranean coastal site: Alicante (Spain). *International Journal of Climatology*, 31(3), 468–486. Available from: <https://doi.org/10.1002/joc.2064>
- Badan Informasi Geospasial. (2018) DEMNAS. Digital Elevation Model (DEM) Nasional.
- Belgaman, H.A., Ichinyanagi, K., Suwarman, R., Tanoue, M., Aldrian, E., Utami, A.I.D. et al. (2017) Characteristics of seasonal precipitation isotope variability in Indonesia. *Hydrological Research Letters*, 11(2), 92–98. Available from: <https://doi.org/10.3178/hrl.11.92>
- Cantero, E., Sanz, J., Borbón, F., Paredes, D. & García, A. (2022) On the measurement of stability parameter over complex mountainous terrain. *Wind Energy Science*, 7(1), 221–235. Available from: <https://doi.org/10.5194/wes-7-221-2022>
- Cenedese, A. & Monti, P. (2003) Interaction between an inland urban Heat Island and a sea-breeze flow: a laboratory study. *Journal of Applied Meteorology and Climatology*, 42(11), 1569–1583. Available from: [https://doi.org/10.1175/1520-0450\(2003\)042<1569:IBAIUH>2.0.CO;2](https://doi.org/10.1175/1520-0450(2003)042<1569:IBAIUH>2.0.CO;2)
- Chang, C.-P., Harr, P.A. & Chen, H.-J. (2005) Synoptic disturbances over the equatorial South China Sea and Western maritime continent during boreal winter. *Monthly Weather Review*, 133(3), 489–503. Available from: <https://doi.org/10.1175/MWR-2868.1>
- Chang, C.-P., Wang, Z., McBride, J. & Liu, C.-H. (2005) Annual cycle of Southeast Asia—maritime continent rainfall and the asymmetric monsoon transition. *Journal of Climate*, 18(2), 287–301. Available from: <https://doi.org/10.1175/JCLI-3257.1>
- Chow, W.T.L. & Roth, M. (2006) Temporal dynamics of the urban heat Island of Singapore. *International Journal of Climatology*, 26(15), 2243–2260. Available from: <https://doi.org/10.1002/joc.1364>
- Clayson, C.A., Brown, J. & NOAA CDR Program. (2016) *NOAA Climate Data Record (CDR) of Sea Surface Temperature - WHOI, Version 2*.
- Crawford, K.C. & Hudson, H.R. (1973) The diurnal wind variation in the lowest 1500 ft in Central Oklahoma. June 1966–may 1967. *Journal of Applied Meteorology and Climatology*, 12(1), 127–132. Available from: [https://doi.org/10.1175/1520-0450\(1973\)012<0127:TDWVIT>2.0.CO;2](https://doi.org/10.1175/1520-0450(1973)012<0127:TDWVIT>2.0.CO;2)
- Darmanto, N.S., Varquez, A.C.G. & Kanda, M. (2017) Urban roughness parameters estimation from globally available datasets for mesoscale modeling in megacities. *Urban Climate*, 21, 243–261. Available from: <https://doi.org/10.1016/j.uclim.2017.07.001>
- Darmanto, N.S., Varquez, A.C.G., Kawano, N. & Kanda, M. (2019) Future urban climate projection in a tropical megacity based on global climate change and local urbanization scenarios. *Urban Climate*, 29, 100482. Available from: <https://doi.org/10.1016/j.uclim.2019.100482>
- Fajber, R., Monahan, A.H. & Merryfield, W.J. (2014) At what time of day do daily extreme near-surface wind speeds occur? *Journal of Climate*, 27(11), 4226–4244. Available from: <https://doi.org/10.1175/JCLI-D-13-00286.1>
- Ferdiansyah, M.R., Inagaki, A. & Kanda, M. (2020) Detection of sea-breeze inland penetration in the coastal-urban region using geostationary satellite images. *Urban Climate*, 31, 100586. Available from: <https://doi.org/10.1016/j.uclim.2020.100586>
- Ferijal, T., Batelaan, O., Shanafield, M. & Alfahmi, F. (2022) Determination of rainy season onset and cessation based on a flexible driest period. *Theoretical and Applied Climatology*, 148, 91–104. Available from: <https://doi.org/10.1007/s00704-021-03917-1>
- Freitas, E.D., Rozoff, C.M., Cotton, W.R. & Dias, P.L.S. (2007) Interactions of an urban heat Island and sea-breeze circulations during winter over the metropolitan area of São Paulo, Brazil. *Boundary-Layer Meteorology*, 122(1), 43–65. Available from: <https://doi.org/10.1007/s10546-006-9091-3>
- Gilliam, R.C., Raman, S. & Niyogi, D.D.S. (2004) Observational and numerical study on the influence of large-scale flow direction and coastline shape on sea-breeze evolution. *Boundary-Layer Meteorology*, 111(2), 275–300. Available from: <https://doi.org/10.1023/B:BOUN.0000016494.99539.5a>
- Grau, A., Jiménez, M.A. & Cuxart, J. (2021) Statistical characterization of the sea-breeze physical mechanisms through in-situ and satellite observations. *International Journal of Climatology*, 41(1), 17–30. Available from: <https://doi.org/10.1002/joc.6606>
- Grimmond, C.S.B. & Oke, T.R. (1999) Heat storage in urban areas: local-scale observations and evaluation of a simple model. *Journal of Applied Meteorology and Climatology*, 38(7), 922–940. Available from: [https://doi.org/10.1175/1520-0450\(1999\)038<0922:HSIUAL>2.0.CO;2](https://doi.org/10.1175/1520-0450(1999)038<0922:HSIUAL>2.0.CO;2)
- Hadi, T.W., Horinouchi, T., Tsuda, T., Hashiguchi, H. & Fukao, S. (2002) Sea-breeze circulation over Jakarta, Indonesia: a climatology based on boundary layer radar observations. *Monthly Weather Review*, 130(9), 2153–2166. Available from: [https://doi.org/10.1175/1520-0493\(2002\)130<2153:SBCOJI>2.0.CO;2](https://doi.org/10.1175/1520-0493(2002)130<2153:SBCOJI>2.0.CO;2)
- Hadi, T.W., Tsuda, T., Hashiguchi, H. & Fukao, S. (2000) Tropical Sea-breeze circulation and related atmospheric phenomena observed with L-band boundary layer radar in Indonesia. *Journal of the Meteorological Society of Japan. Ser. II*, 78(2), 123–140. Available from: https://doi.org/10.2151/jmsj1965.78.2_123
- Hamada, J.-I., Yamanaka, M.D., Matsumoto, J., Fukao, S., Winarso, P.A. & Sribimawati, T. (2002) Spatial and temporal variations of the rainy season over Indonesia and their link to ENSO. *Journal of the Meteorological Society of Japan. Ser. II*, 80(2), 285–310. Available from: <https://doi.org/10.2151/jmsj.80.285>
- Hersbach, H., Bell, B., Berrisford, P., Hirahara, S., Horányi, A., Muñoz-Sabater, J. et al. (2020) The ERA5 global reanalysis.

- Quarterly Journal of the Royal Meteorological Society*, 146(730), 1999–2049. Available from: <https://doi.org/10.1002/qj.3803>
- Hu, X.-M. & Xue, M. (2016) Influence of synoptic sea-breeze fronts on the urban heat Island intensity in Dallas–Fort Worth, Texas. *Monthly Weather Review*, 144(4), 1487–1507. Available from: <https://doi.org/10.1175/MWR-D-15-0201.1>
- Hu, Y., Tan, J., Grimmond, S., Ao, X., Yan, Y. & Liu, D. (2022) Observed and modeled urban Heat Island and sea-breeze circulation interactions: a Shanghai case study. *Journal of Applied Meteorology and Climatology*, 61(3), 239–259. Available from: <https://doi.org/10.1175/JAMC-D-20-0246.1>
- Huffman, G.J., Stocker, E.F., Bolvin, D.T., Nelkin, E.J. & Tan, J. (2019) GPM IMERG Final Precipitation L3 1 month 0.1 degree x 0.1 degree V06.
- Jayakrishnan, P.R., Sivaprasad, P., Nettukandy Chenoli, S., Babu, C.A., Samah, A.A. & Mohammedali, N.P. (2021) Sea breeze characteristics over a coastal station in peninsular Malaysia. *Journal of Earth System Science*, 130(3), 126. Available from: <https://doi.org/10.1007/s12040-021-01632-z>
- Jiang, P., Wen, Z., Sha, W. & Chen, G. (2017) Interaction between turbulent flow and sea breeze front over urban-like coast in large-eddy simulation. *Journal of Geophysical Research: Atmospheres*, 122(10), 5298–5315. Available from: <https://doi.org/10.1002/2016JD026247>
- Jiménez, P.A., de Arellano, J.V.-G., Dudhia, J. & Bosveld, F.C. (2016) Role of synoptic- and meso-scales on the evolution of the boundary-layer wind profile over a coastal region: the near-coast diurnal acceleration. *Meteorology and Atmospheric Physics*, 128(1), 39–56. Available from: <https://doi.org/10.1007/s00703-015-0400-6>
- Junnaedhi, I.D.G.A., Inagaki, A., Varquez, A.C.G. & Kanda, M. (2021) Evaluation of multiple simulated sea-breeze events in tropical megacity using high-temporal-resolution observation data. *Journal of Japan Society of Civil Engineers, Ser. B1 (Hydraulic Engineering)*, 77(2), I_1309–I_1314. Available from: https://doi.org/10.2208/jscejhe.77.2_I_1309
- Masouleh, Z.P., Walker, D.J. & Crowther, J.M. (2019) A long-term study of sea-breeze characteristics: a case study of the Coastal City of Adelaide. *Journal of Applied Meteorology and Climatology*, 58(2), 385–400. Available from: <https://doi.org/10.1175/JAMC-D-17-0251.1>
- Mauder, M., Cuntz, M., Drüe, C., Graf, A., Rebmann, C., Schmid, H.P. et al. (2013) A strategy for quality and uncertainty assessment of long-term eddy-covariance measurements. *Agricultural and Forest Meteorology*, 169, 122–135. Available from: <https://doi.org/10.1016/j.agrformet.2012.09.006>
- Miller, S.T.K., Keim, B.D., Talbot, R.W. & Mao, H. (2003) Sea breeze: structure, forecasting, and impacts. *Reviews of Geophysics*, 41(3), 1–31. Available from: <https://doi.org/10.1029/2003RG000124>
- Mori, S., Hamada, J.-I., Hattori, M., Wu, P.-M., Katsumata, M., Endo, N. et al. (2018) Meridional march of diurnal rainfall over Jakarta, Indonesia, observed with a C-band Doppler radar: an overview of the HARIMAU2010 campaign. *Progress in Earth and Planetary Science*, 5(1), 47. Available from: <https://doi.org/10.1186/s40645-018-0202-9>
- Moron, V., Robertson, A.W. & Boer, R. (2009) Spatial coherence and seasonal predictability of monsoon onset over Indonesia. *Journal of Climate*, 22(3), 840–850. Available from: <https://doi.org/10.1175/2008JCLI2435.1>
- Nitta, T. & Sekine, S. (1994) Diurnal variation of convective activity over the tropical Western Pacific. *Journal of the Meteorological Society of Japan. Ser. II*, 72(5), 627–641. Available from: https://doi.org/10.2151/jmsj1965.72.5_627
- Oke, T.R., Mills, G., Christen, A. & Voogt, J.A. (2017) *Urban Climates*. Cambridge, UK: Cambridge University Press.
- Pinandito, M., Sugondo, S., Sugimoto, N. & Matsui, I. (2001) Long-term lidar observation and analysis of aerosol vertical profiles in Jakarta, Indonesia. In: *Proceedings of the SPIE 4153, Lidar remote sensing for industry and environment monitoring*. Bellingham, WA: SPIE, pp. 191–198.
- Qian, J.-H., Robertson, A.W. & Moron, V. (2010) Interactions among ENSO, the monsoon, and diurnal cycle in rainfall variability over Java, Indonesia. *Journal of the Atmospheric Sciences*, 67(11), 3509–3524. Available from: <https://doi.org/10.1175/2010JAS3348.1>
- Reddy, T.V.R., Mehta, S.K., Ananthavel, A., Ali, S., Annamalai, V. & Rao, D.N. (2021) Seasonal characteristics of sea breeze and thermal internal boundary layer over Indian east coast region. *Meteorology and Atmospheric Physics*, 133(2), 217–232. Available from: <https://doi.org/10.1007/s00703-020-00746-1>
- Reible, D.D., Simpson, J.E. & Linden, P.F. (1993) The sea breeze and gravity-current frontogenesis. *Quarterly Journal of the Royal Meteorological Society*, 119(509), 1–16. Available from: <https://doi.org/10.1002/qj.49711950902>
- Renggono, F., Hashiguchi, H., Fukao, S., Yamanaka, M.D., Ogino, S.-Y., Okamoto, N. et al. (2001) Precipitating clouds observed by 1.3-GHz boundary layer radars in equatorial Indonesia. *Annales Geophysicae*, 19(8), 889–897. Available from: <https://doi.org/10.5194/angeo-19-889-2001>
- Robinson, F.J., Patterson, M.D. & Sherwood, S.C. (2013) A numerical modeling study of the propagation of Idealized Sea-breeze density currents. *Journal of the Atmospheric Sciences*, 70(2), 653–668. Available from: <https://doi.org/10.1175/JAS-D-12-0113.1>
- Roth, M., Sanchez, B., Li, R. & Velasco, E. (2022) Spatial and temporal characteristics of near-surface air temperature across local climate zones in a tropical city. *International Journal of Climatology*, 42(16), 9730–9752. Available from: <https://doi.org/10.1002/joc.7862>
- Schoenberger, L.M. (1984) Doppler radar observation of a land-breeze cold front. *Monthly Weather Review*, 112(12), 2455–2464. Available from: [https://doi.org/10.1175/1520-0493\(1984\)112<2455:DROOAL>2.0.CO;2](https://doi.org/10.1175/1520-0493(1984)112<2455:DROOAL>2.0.CO;2)
- Shen, L., Zhao, C., Ma, Z., Li, Z., Li, J. & Wang, K. (2019) Observed decrease of summer sea-land breeze in Shanghai from 1994 to 2014 and its association with urbanization. *Atmospheric Research*, 227, 198–209. Available from: <https://doi.org/10.1016/j.atmosres.2019.05.007>
- Shen, L., Zhao, C. & Yang, X. (2021a) Insight into the seasonal variations of the sea-land breeze in Los Angeles with respect to the effects of solar radiation and climate type. *Journal of Geophysical Research: Atmospheres*, 126(6), e2020JD033197. Available from: <https://doi.org/10.1029/2020JD033197>
- Simpson, J.E. (1969) A comparison between laboratory and atmospheric density currents. *Quarterly Journal of the Royal Meteorological Society*, 95(406), 758–765. Available from: <https://doi.org/10.1002/qj.49709540609>
- Simpson, J.E. & Britter, R.E. (1979) The dynamics of the head of a gravity current advancing over a horizontal surface. *Journal of Fluid Mechanics*, 94(3), 477–495. Available from: <https://doi.org/10.1017/S0022112079001142>
- Simpson, J.E. & Britter, R.E. (1980) A laboratory model of an atmospheric mesofront. *Quarterly Journal of the Royal Meteorological*

- Society*, 106(449), 485–500. Available from: <https://doi.org/10.1002/qj.49710644907>
- Siswanto, S., van der Schrier, G. & van den Hurk, B. (2022) Observed increase of urban extreme rainfall as surface temperature rise: the Jakarta case. *Journal of the Meteorological Society of Japan. Ser., II*, advpub. Available from: <https://doi.org/10.2151/jmsj.2022-023>
- Sofyan, A., Kitada, T. & Kurata, G. (2007) Characteristics of air pollution transport in Jakarta area in dry season. *Proceedings of the Symposium on Global Environment*, 15, 89–94. Available from: <https://doi.org/10.2208/proge.15.89>
- Sorbjan, Z. & Grachev, A.A. (2010) An evaluation of the flux-gradient relationship in the stable boundary layer. *Boundary-Layer Meteorology*, 135(3), 385–405. Available from: <https://doi.org/10.1007/s10546-010-9482-3>
- Stull, R.B. (1988) *An introduction to boundary layer meteorology*. Dordrecht; Boston: Kluwer Academic Publishers.
- Sumner, G.N. (1977) Sea breeze occurrence in hilly terrain. *Weather*, 32(6), 200–208. Available from: <https://doi.org/10.1002/j.1477-8696.1977.tb04556.x>
- Suwarman, R., Ichianagi, K., Tanoue, M., Yoshimura, K., Mori, S., Yamanaka, M.D. et al. (2013) The variability of stable isotopes and water origin of precipitation over the maritime continent. *Solaiat*, 9, 74–78. Available from: <https://doi.org/10.2151/sola.2013-017>
- Tanaka, M. (1994) The onset and retreat dates of the austral summer monsoon over Indonesia, Australia and New Guinea. *Journal of the Meteorological Society of Japan. Ser., II*, 72(2), 255–267. Available from: https://doi.org/10.2151/jmsj1965.72.2_255
- Varquez, A.C.G., Nakayoshi, M. & Kanda, M. (2015) The effects of highly detailed urban roughness parameters on a sea-breeze numerical simulation. *Boundary-Layer Meteorology*, 154(3), 449–469. Available from: <https://doi.org/10.1007/s10546-014-9985-4>
- Wang, Q., Wang, Y., Fan, Y., Hang, J. & Li, Y. (2019) Urban heat Island circulations of an idealized circular city as affected by background wind speed. *Building and Environment*, 148, 433–447. Available from: <https://doi.org/10.1016/j.buildenv.2018.11.024>
- Wu, P., Hara, M., Fudeyasu, H., Yamanaka, M.D., Matsumoto, J., Syamsudin, F. et al. (2007) The impact of trans-equatorial monsoon flow on the formation of repeated torrential rains over Java Island. *Sola*, 3, 93–96. Available from: <https://doi.org/10.2151/sola.2007-024>
- Yamanaka, M.D. (2016) Physical climatology of Indonesian maritime continent: an outline to comprehend observational studies. *Atmospheric Research*, 178–179, 231–259. Available from: <https://doi.org/10.1016/j.atmosres.2016.03.017>
- Yamanaka, M.D., Ogino, S.-Y., Wu, P.-M., Jun-Ichi, H., Mori, S., Matsumoto, J. et al. (2018) Maritime continent coastlines controlling Earth's climate. *Progress in Earth and Planetary Science*, 5(1), 21. Available from: <https://doi.org/10.1186/s40645-018-0174-9>
- Yang, G.-Y. & Slingo, J. (2001) The diurnal cycle in the tropics. *Monthly Weather Review*, 129(4), 784–801. Available from: [https://doi.org/10.1175/1520-0493\(2001\)129<0784:TDCITT>2.0.CO;2](https://doi.org/10.1175/1520-0493(2001)129<0784:TDCITT>2.0.CO;2)
- Yoden, S., Otsuka, S., Joko Trilaksono, N. & Wahyu, H.T. (2016) Recent Progress in research on the maritime continent monsoon. *The Global Monsoon System*, 9, 63–77.
- Yoshikado, H. (1992) Numerical study of the daytime urban effect and its interaction with the sea breeze. *Journal of Applied Meteorology*, 31(10), 1146–1164. Available from: [https://doi.org/10.1175/1520-0450\(1992\)031<1146:NSOTDU>2.0.CO;2](https://doi.org/10.1175/1520-0450(1992)031<1146:NSOTDU>2.0.CO;2)
- Yoshikado, H. (1994) Interaction of the sea breeze with urban Heat Islands of different sizes and locations. *Journal of the Meteorological Society of Japan. Ser. II*, 72(1), 139–143. Available from: https://doi.org/10.2151/jmsj1965.72.1_139
- Yoshikado, H. & Kondo, H. (1989) Inland penetration of the sea breeze over the suburban area of Tokyo. *Boundary-Layer Meteorology*, 48(4), 389–407. Available from: <https://doi.org/10.1007/BF00123061>

How to cite this article: Junnaedhi, I. D. G. A., Inagaki, A., Ferdiansyah, M. R., & Kanda, M. (2023). Seasonal sea breeze variation analysis based on multi-year near-surface observations in Jakarta, Indonesia. *International Journal of Climatology*, 43(11), 5177–5195. <https://doi.org/10.1002/joc.8139>